RMS Based Health Indicators for Remaining Useful Lifetime Estimation of Bearings

A. Klausen [1] H.V. Khang [1] K.G. Robbersmyr [1]

[1]*Department of Engineering Sciences, Mechatronics Group, University of Agder, N-4879 Grimstad, Norway. E-mail: kjell.g.robbersmyr@uia.no*

Abstract

Estimating the remaining useful life (RUL) of bearings from healthy to faulty is important for predictive maintenance. The bearing fault severity can be estimated based on the energy or root mean square (RMS) of vibration signals, and a stopping criterion can be set based on a threshold given by an ISO standard. However, the vibration RMS is often not monotonically increasing with damage, which renders a challenge for predicting the RUL. This study proposes a novel method for splitting the vibration signal into multiple frequency bands before RMS calculations to generate multiple health indicators. Monotonic health indicators are identified using the Spearman coefficient, and the RUL is afterward estimated for each indicator using a suitable model and parameter update scheme. Historical failure data is not required to set any parameters. The proposed method is tested with the Paris' law, where parameters are updated by particle filters. Experimental results from two test rigs validate the performance of the proposed method.

Keywords: Ball bearings, Remaining useful life, Particle filter, Paris' law, Vibration measurement

1 Introduction

Bearings are widely used in rotating machines, and bearing defects result in increased vibration, temperature, and friction. Up to 44% of failures in the most common motors, namely induction motors, are due to bearing faults Zhang et al. (2011). The vibration from severe bearing faults may damage other machine components, such as gears, stators, and pump seals. Unscheduled stops can cause extended downtimes and huge expenses due to maintenance and productivity losses. Monitoring the bearing health condition is essential to avoid emergency shutdowns and to plan maintenance.

A condition monitoring (CM) system can detect faults and enhance machine reliability. In rotating machines, such systems can detect faults using vibration signals, typically by using the envelope spectrum McFadden and Smith (1984). More advanced methods for fault diagnosis apply machine learning Lu et al.

(2016b), whitening methods Peeters et al. (2017), and minimum entropy deconvolution Abboud et al. (2019). Continued machine operation after detecting the initial bearing fault is beneficial for planning maintenance or even necessary if the machine should halt in a controlled manner. As such, an estimation of the bearing remaining useful life (RUL) is crucial to select between regulated or emergency stop. Here follows a general methodology for estimating the RUL Lei et al. (2018):

1. Produce a health indicator (HI) that correlates to the component wear

2. Divide the HI into multiple health stages (HSs)

3. Identify the transition from the first to the second HS

4. Predict future HI trend using a suitable model

5. Determine the remaining time left, i.e. RUL, until the prediction reaches a failure threshold (FT)

The bearing HI can be assessed by examining the level of wear on the rollers and raceways. However, this wear is impractical to determine, as an offline inspection is required after dissembling the bearing Lei et al. (2018), resulting in productivity loss. Instead, the HI can be estimated using less invasive methods. The vibration signal acquired using an accelerometer is a good substitute, as wear on the rollers or raceways increases the vibration energy Singleton et al. (2017).

HIs can be categorized into physical HIs (PHIs) and virtual HIs (VHIs) Hu et al. (2012). PHIs are generated from primarily physical signals and are directly related to the physics of failure. Examples are the vibration root mean square (RMS) Li et al. (2015), kurtosis Lei et al. (2016b), and characteristic bearing fault frequency amplitudes Gebraeel et al. (2004). On the other hand, VHIs do not correlate directly with the physics of failure Hu et al. (2012) and can be calculated by processing multiple PHIs. The Mahalanobis distance was applied in Wang et al. (2016) to fuse 14 PHIs into a single VHI, and principal component analysis (PCA) was used in Lu et al. (2016a) to estimate the principal component of multiple PHIs.

The bearing degradation can be divided into two or multiple HSs Lei et al. (2018). During the first HS, there is no apparent degradation increase in the vibration signal, while the signal may increase rapidly during proceeding ones Wang (2002). This transition can be detected using baseline measurements of the vibration RMS signal Wang (2002) and kurtosis value Li et al. (2015). For example, the HI mean and standard deviation can be determined during baseline measurements, and a substantial deviation suggests the transition from the first to the second HS.

After transitioning to the second HS, the HI can be predicted with a mathematical model that resembles the failure physics. Analytic models such as the exponential model Li et al. (2015); Wang and Tsui (2017), Brownian motion Wang et al. (2016), and Paris' law Lei et al. (2016a) have been used to model the HI. The Kalman filter (KF) Singleton et al. (2015) and particle filter (PF) Qian and Yan (2015) can be applied to update parameters for the models. Also, numerical optimization can be used to minimize the error between measurements and a model Ahmad et al. (2018).

As an alternative to analytic models, data-driven methods can perform predictions without knowing the physics of failure, such as the Gaussian process model (GPM) Aye and Heyns (2017), least squares support vector machine (LSSVM) Lu et al. (2016a); Manjurul Islam et al. (2021) and transfer learning method applied to a multiple layer perceptron network Zhu et al. (2020). These models are then used to predict the future trend of the HI. However, most data-driven models require training data from previous failures, which may not always be available.

The estimated RUL is the predicted time until the model reaches an FT, hence determining this threshold accurately is essential for the estimation accuracy. For VHIs, historical failure data from a similar setup is often necessary to create a suitable FT Khan et al. (2018); Zhu et al. (2019); Lei et al. (2016a). However, for machines where no historical failure data is available, many of the methods reported in the literature may not be applicable. In Klausen et al. (2018), the FT is set based on the vibration RMS as guided by the ISO standard 10816-3 ISO (1998), without involving historical failure data.

Estimating the RUL using vibration RMS is difficult as this HI does not always increase monotonically with damage. There are methods for extracting the hidden degradation state of a system using phase-space warping Qian et al. (2017). However, the proposed RUL estimation method in Qian et al. (2017) requires setting parameters using historical failure data. Another method Qian and Yan (2015) uses enhanced particle filter to estimate the RUL, but the failure threshold for the RP entropy is set without justification. Artificial intelligence methods, and most particularly deep learning methods, have also been used to estimate the RUL of bearings Akkad and He (2019); Ma and Mao (2019); Wang et al. (2019); Cheng et al. (2020); Pan et al. (2020). However, these methods require supervised learning techniques using historical failure data to train the model. Consequently, there is a challenge in estimating the RUL on systems where historical failure data is not available.

This paper proposes a method to address the challenges above for bearing RUL estimation. The physical meaning of the RUL estimation is preserved by basing the HIs on RMS, and the FTs are based on ISO 10816-3 ISO (1998). Historical failure data is not needed to determine either monotonic VHIs or FTs in the proposed method. The vibration signal is first divided into multiple frequency bands to construct multiple RMS-based HIs. Instead of using a digital filter bank, the proposed approach utilizes only the resulting bins of a discrete Fourier transform (DFT) of the vibration signal. This approach yields no energy loss and is less computationally expensive than digital finite impulse response (FIR) filters. The Spearman coefficient is used to determine which of the HIs are suitable for RUL estimation. FTs for the generated HIs are computed by extending the method in Klausen et al. (2018). Statistically significant changes in each HI are compared to baseline measurements to determine the transition from the first to second HS. For each monotonic HI, the RUL is estimated by projecting the future

trend using a suitable model. The RUL estimation for each trend is then finally combined to a single weighted RUL estimation, that is more accurate than either estimation alone. It should be noted that the proposed method correlates energy increase/decrease to variations in component health, and does not change in operating conditions. Hence, for variable speed/load operations, other changes also need to be considered. Vibration signals from two bearing degradation tests are used to validate the proposed method. PFs are used to update model parameters of the Paris' law to predict the future trend of HIs.

The rest of the paper is organized as follows. Practical differences between velocity- and acceleration-based RMS are discussed in Section 2. Next, the proposed approach for subdividing the vibration signal into multiple RMS HIs is detailed in Section 3. Afterwards, the algorithm used for RUL estimation is presented in Section 4, and the experimental results from two test rigs are given in Section 5. Finally, conclusions are drawn in Section 6.

2 Velocity versus acceleration RMS

ISO Standard 10816-3 ISO (1998) defines levels of velocity-based vibration RMS values for rotating machines with the rating over 15 kW. Four levels are given, ranging between A - D: A = "standard acceptance for new machines"; B = "unlimited operation is possible"; C = "short term operation allowed"; D = "vibration causes damage". A machine should stop before reaching level D. Hence, the boundary between levels C and D can be used as a FT.

The RMS of a sampled vibration signal x can be calculated with

$$\text{RMS}(x) = \sqrt{\frac{1}{n}\sum_{i=1}^{n}x_i^2} \tag{1}$$

where n is the vibration signal length, and x_i is the i'th vibration sample. The vibration signal in this study is measured with an accelerometer, which gives the vibration in acceleration units (m/s^2). Through integration, the *velocity* signal $x_v(t)$ is acquired, which is used for checking vibration severity according to ISO 10816-3 ISO (1998). Before integrating, the vibration signal is filtered with a first-order infinite impulse response (IIR) high-pass filter. The cut-off frequency is set based on shaft speed f_s ISO (1998):

$$\text{Cut-off frequency} = \begin{cases} 10 \text{ Hz} & \text{if } f_s \geq 10 \text{ Hz} \\ 2 \text{ Hz} & \text{if } 10 > f_s \geq 2 \text{ Hz} \end{cases} \tag{2}$$

It should be noted that the standard ISO (1998) does not define a cut-off frequency for shaft frequencies

lower than 2 Hz. Afterwards, the acceleration signal is integrated digitally using the trapezoidal rule:

$$x_{v,i} = \begin{cases} 0 & i = 0 \\ x_{v,i-1} + \frac{x_{i-1}+x_i}{2}\text{d}t & \text{else} \end{cases} \tag{3}$$

where $x_{v,i}$ is the velocity signal at a discrete time step i. The mean value of x_v is finally removed after integration. For brevity, the following notation is used: $R_a = \text{RMS}(x)$ and $R_v = \text{RMS}(x_v)$.

In many practical cases, when monitoring bearing faults, R_v is not suitable for RUL estimation. Initial bearing defects generate high-frequency resonance vibration, and integration reduces the effect of high-frequency components Klausen et al. (2018). For that reason, the acceleration-based RMS value is better suited as an HI. However, the ISO standard ISO (1998) is only defined for a velocity-based RMS signal. To alleviate this limitation, the FT is experimentally transformed into the acceleration domain before estimating bearing RUL. This procedure was proposed in Klausen et al. (2018) and is briefly described in the following paragraph.

The mean velocity and acceleration RMS values are first calculated at a known steady state (baseline) and are denoted as $\bar{R}_v$ and $\bar{R}_a$, respectively. Afterwards, the ratio between the velocity-based FT and the baseline is used to scale the acceleration-based baseline into a suitable threshold $\hat{R}_a$ using

$$\hat{R}_a = \frac{\hat{R}_v}{\bar{R}_v}\bar{R}_a \tag{4}$$

where the value of $\hat{R}_v$ is taken from the ISO standard.

Vibration data collected by the NSF I/UCR Center for Intelligent Maintenance Systems (IMS) Qiu et al. (2006) is used as a numerical example of this calculation. Four Rexnord ZA-2115 double row bearings are run to failure by applying a constant load of 26.6 kN at a constant speed of 2000 revolutions per minute (rpm). The test is stopped when the circulating oil is thoroughly contaminated with metal debris. Every 10 minutes, 1 second of vibration data was measured on each bearing housing with a sample rate of 20480 Hz. An index k is defined to keep track of which 1-second vibration signal is in use. Accelerometer data from the second run-to-failure test, consisting of 982 vibration measurements, are used to calculate the acceleration-based failure threshold. An outer race fault was observed in bearing number 1 after this test.

The first 30 hours of vibration data ($k \in [1, 180]$ vibration signals) are used as a baseline, and the mean RMS values are $\bar{R}_a = 0.757$ m/s^2 and $\bar{R}_v = 0.755$ mm/s. The motor size is assumed smaller than 15 kW, and therefore the FT is set slightly lower than level D
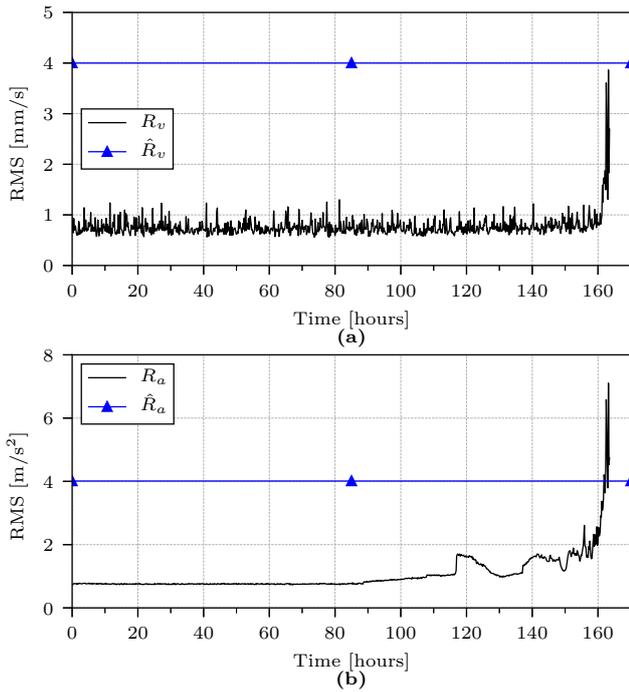
Figure 1: Comparison between velocity- and acceleration-based RMS for the IMS dataset. (a) velocity-based RMS and its FT; (b) acceleration-based RMS and its FT.

in the ISO standard ISO (1998), at $\hat{R}_v = 4$ mm/s. Using (4) results in $\hat{R}_a = 4.01$ m/s^2. Fig. 1 (a) shows R_v and $\hat{R}_v$, while Fig. 1 (b) shows R_a and the resulting FT $\hat{R}_a$. As observed in Fig. 1 (a), R_v starts increasing from the mean value near the end of useful life ($t \approx$ 160 hours), giving a short time to stop the machine and plan maintenance. However, R_a starts increasing much sooner ($t \approx 90$ hours), which better allows for predicting RUL and plan maintenance. The two trends reach their respective FTs near the end of life, which shows that the transformation can be used for this purpose.

R_a in Fig. 1 (b) is, however, not suitable for RUL estimation due to non-monotonic oscillations. For example, the sudden increase of R_a at $t \approx 117$ hours, and the subsequent decrease, render a challenge for determining the actual degradation trend. A more stable HI should be extracted from the vibration signal to achieve better RUL estimation. In the next section, a new approach for extracting more useful RMS data from the vibration signal is proposed.

3 Proposed RMS health indicator

3.1 Filter bank RMS

A digital filter bank can be used to subdivide a signal into multiple components, where each component contains a frequency sub-band of the signal. The filter bank can be created by iteratively passing the signal through a low- and high-pass FIR filter and decimating each output signal to half the signal frequency. Such a procedure has some drawbacks: Digital FIR filters use kernel convolution to filter the signal, and only the overlapping part between the filter kernel and the signal should be preserved to avoid adding signal artifacts. A high order FIR filter kernel would then remove much of the signal energy, and the loss is exponential for each level of filtering. However, a low order FIR filter kernel results in a considerable frequency overlap between the signal components. Computing a digital filter bank is also computationally taxing if the input signal is long, and multiple frequency levels are required. Such a filter-bank is, however, not required to calculate the RMS in different frequency regions. The following explains how the vibration RMS in a particular frequency band can be determined with the DFT spectrum bins.

An alternative representation of RMS is given by the energy E of the signal, such as

$$\text{RMS}(x) = \sqrt{\frac{\text{E}(x)}{T}} \qquad (5)$$

where T is the vibration signal length in seconds. The signal energy can be calculated in both time and frequency domain with

$$\text{E}(x) = \sum_{i=1}^{n} |x_i|^2 \Delta t, \qquad \text{E}(X) = \sum_{i=1}^{n} |X_i|^2 \Delta f \quad (6)$$

where Δt is the vibration sampling period, $X = (X_1, \ldots, X_n)$ is the DFT, and Δf is the frequency step between each DFT bin.

To explain the procedure, the DFT is assumed ordered from 0 Hz to Nyquist frequency, and from negative Nyquist up to 0 Hz. Let $X_L = (X_{LP}, Z_{n/2}, X_{LN})$, where X_{LP} contains the DFT values of the lower positive frequencies (i.e. 0 Hz to half the Nyquist frequency), $Z_{n/2}$ contains $n/2$ zeros, and X_{LN} contains the DFT values of the lower negative frequencies. Similarly, let $X_H = (Z_{n/4}, X_{HP}, X_{HN}, Z_{n/4})$, where X_{HP} and X_{HN} are the DFT values of higher positive and negative frequencies, respectively. This arrangement represents a single level filter bank that splits X at half Nyquist frequency completely. Because of the added zeros in the array, the two components X_H and X_L can be directly summed element-wise to re-create X.

The total energy can afterwards be calculated as

$$\text{E}(X) = \text{E}(X_L + X_H) = \sum_{i=1}^{n} |X_{L,i} + X_{H,i}|^2 \Delta f \quad (7)$$

where $X_{L,i}$ and $X_{H,i}$ are the i'th bin of X_L and X_H, respectively. Let the spectrum bins be given by their complex values, i.e. $X_{L,i} = a_{L,i} + jb_{L,i}$, $X_{H,i} = a_{H,i} + jb_{H,i}$, then (7) becomes

$$\text{E}(X) = \sum_{i=1}^{n} |a_{L,i} + a_{H,i} + j(b_{L,i} + b_{H,i})|^2 \Delta f \quad (8)$$

$$= \sum_{i=1}^{n} \left(a_{L,i}^2 + 2a_{L,i}a_{H,i} + a_{H,i}^2 \right.$$
$$\left. + b_{L,i}^2 + 2b_{L,i}b_{H,i} + b_{H,i}^2 \right) \Delta f \quad (9)$$

Given that X_L and X_H represent a complete signal separation at half Nyquist frequency, the overlap between X_L and X_H is zero. Hence, $2a_{L,i}a_{H,i} = 2b_{L,i}b_{H,i} = 0$, and (9) is reduced to

$$\text{E}(X) = \sum_{i=1}^{n} (a_{L,i}^2 + a_{H,i}^2 + b_{L,i}^2 + b_{H,i}^2) \Delta f$$

$$= \sum_{i=1}^{n} (|a_{L,i} + jb_{L,i}|^2) \Delta f$$

$$+ \sum_{i=1}^{n} (|a_{H,i} + jb_{H,i}|^2) \Delta f$$

$$= \text{E}(X_L) + \text{E}(X_H) \quad (10)$$

Eq. (10) shows that the energy of the entire signal can be calculated by the energy of separate DFT bins. In effect, the RMS value within a particular frequency band can be calculated directly from the DFT, without any loss of energy. This information is used to split the vibration signal into equally-sized frequency bands and calculate the RMS value for each of them using

$$R_i = \text{RMS}(X_{b,i}) = \sqrt{\frac{E(X_{b,i})}{T}} \quad (11)$$

where $X_{b,i}$ contains the DFT bins within frequency band i. Since the energy of each frequency band can be summed to the total vibration energy, the same applies for RMS such that

$$\text{RMS}(X) = \sqrt{\sum_{i=1}^{N_b} R_i^2} \quad (12)$$

where N_b is the number of equally-sized frequency bands.

In summary, the DFT X is first obtained for the entire vibration signal x at time index k, and afterward,

the energy of bins belonging to frequency band i is used to calculate $R_{i,k}$ using (11). The next step is to obtain FTs for all R_i.

3.2 Filter bank RMS failure thresholds

To get an FT for each R_i, (12) is reconsidered such that

$$\hat{R}_a = \sqrt{\sum_{i=1}^{N_b} \hat{R}_i^2} \quad (13)$$

where $\hat{R}_i$ is the FT defined for R_i. To solve (13) for any number of frequency bands, it is necessary to make some assumptions about the vibration signal. It is assumed that the RMS values can be modeled as normally distributed noise with a mean value μ_i and standard deviation σ_i during baseline measurements, such that

$$R_i^{\text{baseline}} \sim \mathcal{N}(\mu_i, \sigma_i^2) \quad (14)$$

Bearing wear increases vibration energy at the resonance frequencies of the bearing and the machine itself. There are possibly many resonance regions on a rotating machine Klausen et al. (2017b), hence the increased energy spreads over multiple R_i's. Some frequency bands may have relatively high energy before bearing wear, while others have low ones. Therefore, the FTs are based on scaling from the initial baseline value. It is also assumed that this energy increase from bearing wear is proportional to the baseline value of R_i. With these assumptions, the FTs are defined as

$$\hat{R}_i = m\mu_i \quad (15)$$

where m is the constant scaling factor. To determine m, the conservation of energy is considered, such that $\hat{R}_i$ in (15) is substituted into (13) resulting in

$$\hat{R}_a = \sqrt{\sum_{i=1}^{N_b} (m\mu_i)^2} \quad (16)$$

$$\hat{R}_a^2 = m^2 \sum_{i=1}^{N_b} \mu_i^2 \quad (17)$$

Eq. (17) is finally solved for m as

$$m = \sqrt{\hat{R}_a^2 \left/ \sum_{i=1}^{N_b} \mu_i^2 \right.} \quad (18)$$

With the acquired m, the resulting FTs for each RMS band are determined with (15).

The rest of this section contains an example of the proposed RMS filter bank. The IMS dataset introduced in Section 2 is subdivided into equally sized
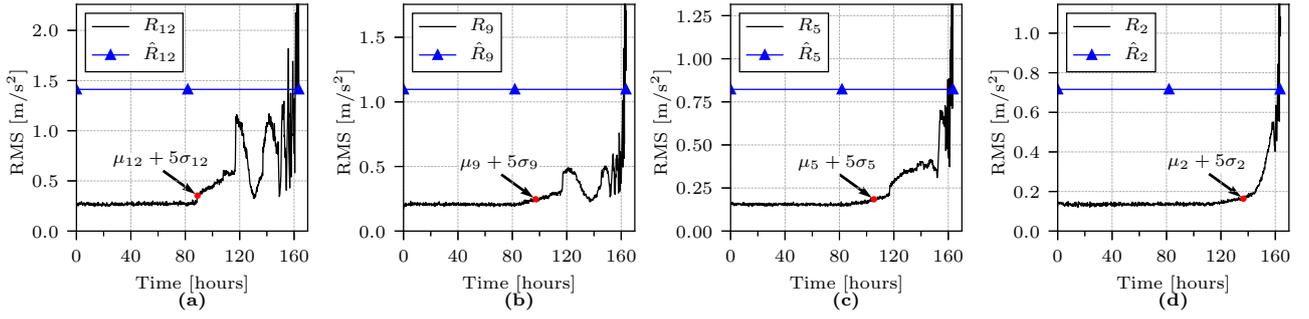
Figure 2: Collection of RMS trends with FTs for the IMS dataset. (a) R_{12} [4400, 4800] Hz; (b) R_9 [3200, 3600] Hz; (c) R_5 [1600, 2000] Hz; (d) R_2 [400, 800] Hz.

bands with 400 Hz bandwidth ($N_b = 25$), and R_i is calculated for each band using (11). The mean value and standard deviation of each R_i are calculated using the baseline vibration values within the first 30 hours ($k \in [1, 180]$). With these values, the FTs for each R_i are calculated using (15) after determining m with (18). Additionally, the initial degradation alarm is triggered at time index $k_{d,i}$ when $R_{i,k_{d,i}} > \mu_i + 5\sigma_i$ Qian et al. (2014).

Fig. 2 shows four RMS trends acquired from different frequency ranges. Fig. 2 (a) shows R_{12}, containing RMS from frequency band [4400, 4800] Hz, and the oscillations are similar to R_a shown in Fig. 1 (b). On the other hand, R_2 ([400, 800] Hz) in Fig. 2 (d) is monotonically increasing after the initial alarm is triggered, thus suitable for RUL estimation. The two other RMS trends in Figs. 2 (b) and (c) share similarities with the two other trends. R_{12} triggers the initial degradation alarm first, i.e., the transition from the first to second HS. This observation supports the model that initial bearing damage is the most prominent in the high-frequency region. Further, the FTs, shown as blue lines, are reached near the end of useful life, and are therefore considered appropriate for RUL estimation. However, it is not simple to know which frequency band is best suited for RUL estimation beforehand. The next section details how suitable RMS trends can be selected online and used to estimate the RUL.

3.3 Spearman coefficient

The Spearman correlation coefficient Spearman (1904) is a rank-based correlation between two signals, being used to describe how monotonic a signal is over time. The Spearman coefficient between a signal x and time t is calculated as

$$\text{Spearman}(x, t) = \frac{\text{cov}(\text{rank}(x), \text{rank}(t))}{\text{STD}(\text{rank}(x))\text{STD}(\text{rank}(t))} \quad (19)$$

where $\text{cov}(\cdot, \cdot)$ is the covariance of two trends, $\text{rank}(\cdot)$ is the rank of a signal, and $\text{STD}(\cdot)$ is the standard deviation. The running Spearman coefficient for R_i at time index k is defined as

$$\rho_{i,k} = \begin{cases} \text{Spearman}(R_{i,k_{d,i}:k}, t) & \text{if } k > k_{d,i} \\ 0 & \text{else} \end{cases} \quad (20)$$

where $R_{i,k_{d,i}:k} = (R_{i,k_{d,i}}, \ldots, R_{i,k})$. Eq. (20) is used to continually check whether R_i increases monotonously over time. The next section describes how to identify monotonic RMS trends.

3.4 RMS trend selection

The Spearman coefficient is used to describe the monotonicity of RMS trends. These values are used to determine which of the RMS trends are useful for RUL estimation. Three criteria must be met by a certain R_i at time index k to be used for RUL estimation:

1. $k \geq k_{d,i} + n_s$, where n_s is the minimum number of samples used to calculate the Spearman coefficient.

2. $\rho_{i,k} \geq \hat{\rho}$, where $\hat{\rho}$ is the Spearman threshold.

3. $i < \min(I_p)$, where I_p is a set of indices i belonging to R_i trends previously passing these criteria. I_p initially starts as an empty list.

The reasons for these criteria are as follows. 1) Several samples are necessary to calculate a stable Spearman coefficient, and n_s is set as the minimum number of samples. In practice, n_s should be based on the number of samples acquired within a time frame significantly shorter than the assumed time from initial fault until breakdown. This time should be estimated based on the bearing load and shaft speed. 2) The running Spearman coefficient must be higher than the threshold $\hat{\rho}$ to accept monotonic trends. The threshold should be at least 0.5 to capture most of the monotonic trends,

Figure 3: Flowchart of the proposed method. The stapled line indicates the proposed method for identifying monotonic RMS trends and calculating the weighted RUL.

even if the signal-to-noise ratio is low. This value can be set higher to track fewer, more influential trends. 3) Bearing energy increases more in low-frequency bands during advanced fault stage, as can be evidenced since R_v in Fig. 1 (a) increases rapidly near the end of useful life. In effect, it is assumed that RMS trends of high-frequency bands trigger the initial degradation alarm first, and the energy increases at low-frequency bands later. The index i of new trends must be smaller than all the other trends previously passing these three criteria since they add more useful information during advanced bearing fault stage. The next section describes how the RUL estimation from multiple RMS trends can be combined.

3.5 Remaining useful lifetime estimation

The RUL is estimated after capturing each vibration signal. There are many reported methods in the literature for tracking a monotonic trend and determining the time until failure by forward propagating a degradation model, such as the Paris' crack propagation model. When a new RMS trend passes the criteria to be tracked, the RUL is estimated using the designated model for this trend. The estimated RUL is here assumed probabilistic to comply with PFs and KFs. Let $p(l_{i,k} \mid R_{i,k_{d,i}:k})$ denote the probability density function (PDF) of RUL estimation $l_{i,k}$ for RMS trend i at time index k. Most of the methods reported in literature only track a single trend over time, and only estimate the RUL once per new vibration signal. In contrast, the proposed method allows for tracking up to N_b trends and estimating the RUL for each of

them. There is an opportunity to combine multiple estimations into a single, more accurate estimation. The next subsection shows how these RUL estimations can be combined by utilizing the Spearman coefficient as a weight.

3.6 Weighted remaining useful lifetime

The vibration signal is split into N_b frequency bands, where each band is used to calculate R_i. Theoretically, up to N_b trends can be monitored, and all RUL estimations should be used in a weighted decision. Since monotonic trends are better suited for RUL estimation, these get a higher weight. Then, let the weight of each R_i be

$$W_{i,k} = \left(\rho_{i,k}^3 - \rho_L^3 \right) / \left(1 - \rho_L^3 \right) \quad (21)$$

where the Spearman coefficient is cubed to prioritize monotonic trends, and ρ_L is a limiting value.

Afterwards, the weighted RUL $\bar{l}_k$ PDF at time index k is defined as

$$p(\bar{l}_k \mid R_{1:N_b}) = \sum_{i=1}^{N_b} W_{i,k}\, p(l_{i,k} \mid R_{i,k_{d,i}:k}) \quad (22)$$

where $R_{1:N_b} = (R_1, \ldots, R_{N_b})$. Operators can monitor the median and confidence intervals (CIs) of $p(\bar{l}_k \mid R_{1:N_b})$ over time.

3.7 Overview

A flowchart of the proposed method is shown in Fig. 3. First, a vibration sensor is installed on the rotating machine, and baseline measurements are made. Based on

ISO 10816-3 ISO (1998), the velocity threshold is set. Using baseline data, the vibration failure threshold $\hat{R}_a$ and thresholds for all RMS bands $\hat{R}_i$ are determined.

Afterwards, new measurements are split into multiple RMS-based HI trends $R_i \ \forall i \in [1, N_b]$. For each trend, the running Spearman coefficient $\rho_{i,k}$ is calculated and checked for monotonicity. If the trend passes the criteria for being monotonic, a new model is initialized. If it is already initialized, the model parameters are updated, and the RUL is estimated. Once all trends are checked, the weighted RUL estimation $p(\bar{l}_k \mid R_{1:N_b})$ is determined, and related statistics can be monitored over time.

3.8 Number of frequency bands

Setting N_b requires some considerations. A high number of bands results in a threshold $\hat{R}_a$ divided on a large number of RMS trends $\hat{R}_i$. Consequently, there is a higher chance that a few of these trends increase by more than others. Thus, setting a high number of N_b may result in a more conservative RUL estimation as some R_i may pass the threshold faster. Besides, a larger number of monotonic trends may need to be tracked using parameter update schemes. Thus, there is a potential increased computational load by increasing the number of bands. On the other hand, setting a too low number for N_b may limit the ability to identify frequency bands with monotonic energy increase, restricting the ability to estimate the RUL. N_b should be in the range [20, 40] to strike a balance between the RUL estimation ability and computational burden.

3.9 Robustness against noise

In reality, measurements are always contaminated by noise, and increased noise will increase the signal energy. With increased signal energy during baseline measurements, the gap between the baseline mean and ISO threshold is reduced. Increased noise in the time domain may make the RUL estimation more conservative by decreasing the needed energy to classify the system as damaged.

If the noise is manifested in the energy domain, i.e., the energy fluctuates between measurements such that σ_i increases, the initial degradation alarm is activated at a later stage. Such a change would not affect the failure threshold since $\hat{R}_i$ is only based on the mean value of R_i during baseline measurements, which would not be affected by uniform noise. Besides, the experimental results in this paper are not from simulated data, but rather from real sensor data of two test rigs, including both mechanical and measurement noises.

4 Application with prediction model

This section describes the implementation of a PF used to update parameters of a Paris' crack propagation model Lei et al. (2016a). Combined with the proposed method, this implementation is applied to test the RUL estimation capabilities on vibration data from two experimental tests.

4.1 Degradation model

The bearing degradation level is assumed monotonously increasing and never self-healing. Also, as an increasing number of defects develop in the bearing, the vibration level increases, resulting in an exponential degradation rate. A study Rycerz et al. (2017) shows that bearing crack propagation may be modeled with the Paris' law Paris and Erdogan (1963). This model describes the crack propagation rate in materials under cyclic load, and is given by

$$\frac{\mathrm{d}a}{\mathrm{d}n_c} = c(\Delta k)^m, \qquad \Delta k = \gamma \Delta\sigma\sqrt{\pi a} \qquad (23)$$

where a is the crack size, n_c is the cycle number, c, m and γ are the material constants, and $\Delta\sigma$ is the cyclic load amplitude. Henceforth, a will be referred to as the health state of the bearing. For convenience, let $\alpha = c(\gamma\Delta\sigma\sqrt{\pi})^m$ and $\beta = m/2$, then the modified Paris' law is Lei et al. (2016a)

$$\frac{\mathrm{d}a}{\mathrm{d}n_c} = \alpha a^\beta \qquad (24)$$

Eq. (24) is afterwards re-written in the form of a state-space model as Lei et al. (2016a)

$$\begin{cases} a_k & = a_{k-1} + \alpha_{k-1}a_{k-1}^\beta \Delta n_c \\ \alpha_k & = \alpha_{k-1} \\ R_{i,k} & = a_k + \nu_h \end{cases} \qquad (25)$$

where a_k is the health state at time index k, $\alpha_{k-1} \sim \mathcal{N}(\mu_\alpha, \sigma_\alpha^2)$ is a normally distributed random variable, β is a constant, Δn_c is the number of cycles since last update and $\nu_h \sim \mathcal{N}(0, \sigma_h^2)$ is the measurement noise. The health state a_k is hard to determine in practice and is generally represented with an HI An et al. (2013). Each RMS trend serves as the health state in this paper, which is contaminated by measurement noise. Since the measurement noise is generally small An et al. (2013), a_k can be approximated by $R_{i,k}$.

A PF is applied to update the model parameters based on new samples, but the initial values are set first. The modified Paris' law in (25) has five unknown parameters $(a_1, \mu_\alpha, \beta, \sigma_\alpha^2, \sigma_h^2)$, which must be identified.

4.2 Initial parameter setting

Three model parameters $\Theta_1 = (a_1, \mu_\alpha, \beta)$ are identified by minimizing an objective function using non-linear least squares (NLS). The objective function is the mean square error between measurements and model simulation. Let the measurement available for optimization be $H_{1:n_o} = (R_{i,k-k_{d,i}}, \ldots, R_{i,k})$. To obtain the objective function, the ordinary differential equation in (24) is first solved for a as

$$a = (C_1(1-\beta) + \alpha n_c(1-\beta))^{1/(1-\beta)}, \quad \beta \neq 1 \quad (26)$$

where C_1 is based on the initial conditions, being determined by solving (26) with initial values $a = a_1$ and $n_c = 0$. After the substitution of C_1, the equation becomes

$$P(n_c, \Theta_1) = a = \left(\alpha n_c(1-\beta) + a_1^{1-\beta}\right)^{1/(1-\beta)} \quad (27)$$

Then, the goal is to minimize the error between the measurements and the model, which is given by

$$f(H_j, n_c, \Theta_1) = H_j - P(n_c, \Theta_1) \quad (28)$$

The unknown parameters Θ_1 are finally identified using the NLS minimization routine as described below

$$\underset{\Theta_1}{\arg\min} \, F(H, \Theta_1) \quad (29)$$

$$\text{subject to} \begin{cases} 0 \leq a_1 \leq \max(H_{1:n_o}) \\ 0 \leq \mu_\alpha \leq \infty \\ 0.5 \leq \beta \leq 1.25 \end{cases} \quad (30)$$

$$\text{where } F(H, \Theta_1) = \frac{1}{2} \sum_{j=1}^{n_o} f(H_j, (j-1)\Delta T, \Theta_1)^2 \quad (31)$$

Note that the constraints for β are set to avoid an unstable exponential rate, and the number of cycles is replaced by time with $(j-1)\Delta T$ where ΔT is the time period between vibration measurements (i.e. between each k index). The trust region reflective algorithm Branch et al. (1999) is used in this research to minimize (29).

The variances $\Theta_2 = (\sigma_\alpha^2, \sigma_h^2)$ are set based on baseline data and initial values in Θ_1. The measurement noise variance σ_h^2 is simply identified as the variance of R_i during the baseline measurements, i.e. $\sigma_h^2 = \sigma_i^2$. The process noise heavily influences a PF, and a greater variance results in a wider search space of the PF. The mean value μ_α is here used as the variance, such that $\sigma_\alpha^2 = \mu_\alpha^2$. The next section describes the PF used for updating the Paris' law parameters online.

4.3 Particle filter

After initializing the model parameters, a sequential importance sampling (SIS) PF is applied to further update the parameters. General PF theory is given in Lei et al. (2016a); An et al. (2013); Arulampalam et al. (2002). A set of initial particles $z_k^j \, \forall j \in [1, N_p]$ are initialized at time index k with

$$z_k^j \sim \mathcal{N}\left(\begin{bmatrix} a_{init} \\ \mu_\alpha \end{bmatrix}, \begin{bmatrix} \sigma_h^2 & 0 \\ 0 & \sigma_\alpha^2 \end{bmatrix}\right) \quad (32)$$

where N_p is the number of particles and $a_{init} = P(n_o, \Theta_1)$. The particle weights are initialized as $w_k^j = 1/N_p$.

The next model state is predicted using the particles with

$$z_k^j = \begin{bmatrix} a_k^j \\ \mu_\alpha^j \end{bmatrix} = \begin{bmatrix} a_{k-1}^j + (\mu_\alpha^j + \nu_{\alpha,k})(a_{k-1}^j)^\beta \Delta T \\ \mu_\alpha^j \end{bmatrix} \quad (33)$$

where $\nu_{\alpha,k}^j \sim \mathcal{N}(0, \sigma_\alpha^2)$ is the process noise added due to the uncertainty of bearing load.

The health state a_k is approximated with the RMS trend which is the observed variable. When a new measurement $R_{i,k}$ is available, the particle weights are updated and normalized with

$$\tilde{w}_k^j = w_{k-1}^j p(R_{i,k} \mid z_k^j) \quad (34)$$

$$w_k^j = \tilde{w}_k^j \left/ \sum_{j=1}^{N_p} \tilde{w}_k^j \right. \quad (35)$$

where $\tilde{w}_k^j$ is the un-normalized particle weight and

$$p(R_{i,k} \mid z_k^j) = \frac{1}{\sqrt{2\pi\sigma_h^2}} \exp\left[-\frac{(R_{i,k} - a_k^j)^2}{2\sigma_h^2}\right] \quad (36)$$

A re-sampling step is performed if necessary to deal with particle degeneracy. The effective number of particles is determined with

$$N_{\text{eff}} = 1.0 \left/ \sum_{i=1}^{N_p} w_k^j \right. \quad (37)$$

When $N_{\text{eff}} < N_p/2$, particles are re-sampled according to a systematic re-sampling approach, and particle weights are re-initialized as $w_k^j = 1/N_p$ Hol et al. (2006).

A Gaussian importance re-sampling step is added to lessen particle impoverishment An et al. (2019). If there are less than $N/3$ unique particles after the systematic re-sampling step, all particles are re-drawn from a continuous Gaussian distribution such that

$$z_k^j \sim \mathcal{N}(\mu_p, p\Sigma_p)) \quad (38)$$

where μ_p and Σ_p are the mean and covariance matrix of the particle states, respectively, and p is a scalar greater than 1.0.

The RUL estimated by particle j at time index k is given by

$$l_k^j = \inf\{l_k^j : a^j(l_k + t_k) \geq \hat{R}_i \mid a_{1:k}^j\} \qquad (39)$$

where $a^j(l_k+t_k)$ is the predicted state value for particle j at time $t_k + l_k$ and $a_{1:k}^j = (a_1^j, \ldots, a_k^j)$. To solve (39), the state of each particle j is simulated using the state transition function given by (33) up to the time t_k when $a^j(l_k + t_k) \geq \hat{R}_i$. With the estimated RUL and weight for each particle, the RUL PDF is approximated by

$$p(l_k \mid R_{i,1:k}) = \sum_{j=1}^{N_p} w_k^j \delta(l_k - l_k^j) \qquad (40)$$

where $\delta()$ is the delta-dirac function. The next section includes experimental results using the proposed method combined with the PF for estimating the RUL.

5 Experimental results

5.1 Test rig 1

To validate the proposed method, the IMS bearing dataset Qiu et al. (2006) is utilized. Details of the datasets are given in Section 2. The vibration spectrum of each file is split into evenly sized bands of 400 Hz, giving a total of $N_b = 25$ RMS trends. The baseline measurements are calculated using data from the first 30 hours. It is assumed that the bearing can last for at least 5 hours after the initial fault. Hence the minimum number of samples for Spearman calculation is determined based on this. Given there are 6 files measured per hour, $n_s = 30$. The minimum value of Spearman is set as $\hat{\rho} = 0.9$ to monitor mostly monotonic trends. Non-monotonic trends should not contribute significantly to the weighted RUL. Thus $\rho_L = 0.7$ is the lower Spearman threshold. $N_p = 1000$ particles are used in each PF. To make sure the initial parameters of the PFs are determined based on monotonically increasing values, the number of values for optimization is set to $n_o = n_s$. The value for p in the Gaussian re-sampling step is set to $p = 2$ in an attempt to decrease particle degeneracy.

Fig. 4 shows the results of using the proposed method on this dataset. Subplots in the first column show the identified monotonic RMS trends and the output of the initialized PF. The median and 95% CI of the initialized PF output are shown as red and red-stapled lines, respectively, and black lines show R_i. The blue lines indicate the FT $\hat{R}_i$. Each row in Fig. 4 corresponds to a single index of i, which is shown in the upper left corner of the leftmost subplot column. The second column shows the median and 95% CI of the μ_α parameter. When the median and 95% CI of μ_α

Table 1: Initial PF parameter values for test rig 1 experiment.

i	μ_α	σ_α^2	σ_h^2	β
12	$4.63 \cdot 10^{-6}$	$2.39 \cdot 10^{-12}$	$1.02 \cdot 10^{-4}$	0.5
9	$3.17 \cdot 10^{-6}$	$1.11 \cdot 10^{-12}$	$5.57 \cdot 10^{-5}$	0.96
5	$1.08 \cdot 10^{-5}$	$1.30 \cdot 10^{-11}$	$2.47 \cdot 10^{-5}$	1.25
2	$8.72 \cdot 10^{-6}$	$8.44 \cdot 10^{-12}$	$3.29 \cdot 10^{-5}$	1.25

are practically equal, the converged PF output is estimated and shown in column 3. Initial PF parameters are given in Table 1.

At $t \approx 97$ hours (k = 585), a new PF is initialized for R_{12}, indicating a change in bearing health. This RMS trend, shown in Fig. 4 (a), is from a high-frequency band [4400, 4800] Hz. Initially, R_{12} increases monotonously, but at $t \approx 117$ hours, the trend increases and decreases cyclically. This causes the running Spearman calculation to decrease in value, and the trend loses its significance in RUL estimation. μ_α has converged at $t \approx 110$ hours as seen in Fig. 4 (b), and the estimated trend will continue until the end of RUL. Fig. 4 (c) shows the median and 95% CI output of PF_{12} when μ_α converges. The future trend of the PF suggests an earlier failure than reality. However, the RUL estimated by this trend is not the only contribution to the weighted RUL in the proposed method. Other monotonic RMS trends also contribute to the weighted RUL decision. A vertical black line in Fig. 4 (a) shows when the running Spearman value is less than the requirement of 0.7. At this time, the trend is determined to be unsuitable for RUL estimation after all, and its weight W_{12} is 0 as defined by (21).

R_9 passes the criteria for RUL estimation at $t \approx 110$ hours, and the initial output of the PF is shown in Fig. 4 (d). The parameter μ_α in PF_9 also converges as indicated in Fig. 4 (e). After this time, the converged PF output trend continues until the Spearman coefficient value goes below 0.7 at $t \approx 135$ hours. The converged output of PF_9 is shown in Fig. 4 (f). The converged PF gives a non-conservative RUL estimation, as the value undershoots the FT.

At $t = 115$ hours, PF_5 is initialized, and the initial output is shown in Fig. 4 (g). R_5 has fewer oscillations than the two previously identified RMS trends, and therefore the Spearman coefficient never gets below 0.7. The parameter μ_α converges over 10 hours as shown in Fig. 4 (h), and results in a lower value of μ_α, which gives a less conservative RUL estimation compared to the initial estimation. The predicted output after convergence shown in Fig. 4 (i) will reach the threshold a bit early, but is relatively accurate.

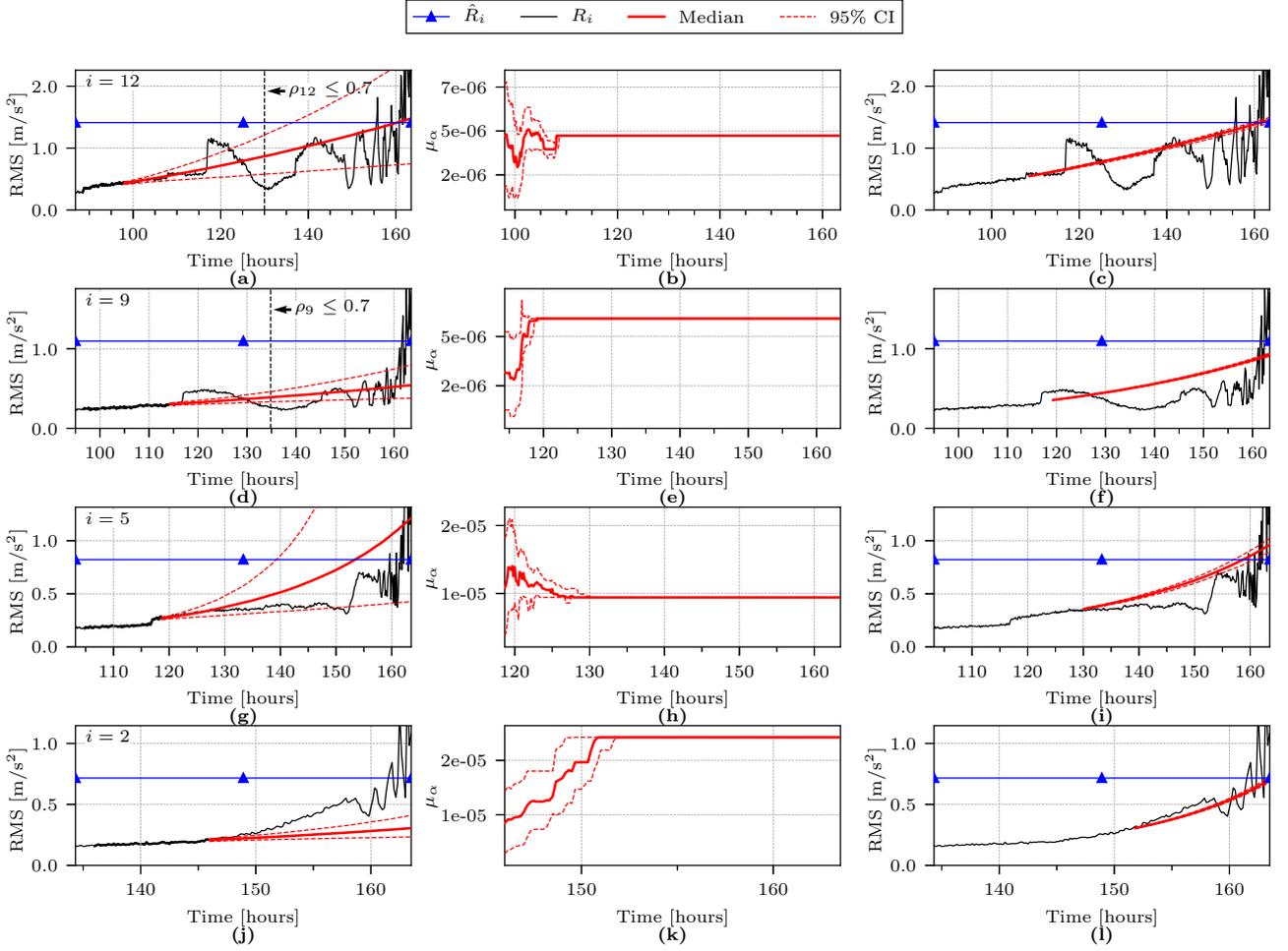When $t \approx 145$ hours, PF_2 is initialized, and R_2 to-

Figure 4: Identified RMS trends, and output of the corresponding PFs. Rows 1-4 indicate $i = [12, 9, 5, 2]$. (column 1) R_i, FT $\hat{R}_i$, and median and 95% CI of initial PF output; (column 2) μ_α over time for the initiated PF; (column 3) predicted PF trend when μ_α converges.

gether with the PF output are shown in Fig. 4 (j). R_2 is the most monotonic trend thus far, but the initial PF is undershooting the FT and initially gives a poor RUL estimation. However, the median and 95% CI of μ_α is continually increasing as seen in Fig. 4 (k) because of the Gaussian re-sampling step. Once the PF has converged at about $t \approx 151$ hours, the PF output in Fig. 4 (l) is following the future trend well, and reaches the FT at almost the correct time.

Combining the RUL estimations of each PF will give a better estimate of the actual RUL. The median of this combined discrete RUL PDF, however, can only take discrete values that are present in the PDF. Consequentially, the median cannot take a value in between two large discrete PDFs. To alleviate this constraint, and to reduce instability, the weighted mean RUL es-

timate is defined as

$$\text{Weighted mean}(k) = \frac{\sum_{i=1}^{N_b} W_{i,k} \sum_{j=1}^{N_p} w_{i,k}^j l_{i,k}^j}{\sum_{i=1}^{N_b} W_{i,k} \sum_{j=1}^{N_p} w_{i,k}^j} \quad (41)$$

which can be a number in between discrete values of the weighted RUL PDF.

The weighed RUL mean, 95% CI and 30% error bars for this dataset are shown in Fig. 5 (a). Here, the true RUL is shown as a solid black line, while the weighted mean and 95% CIs are the red and red-stapled lines, respectively. The 30% error is assumed as an acceptable limit for checking the performance of the RUL estimation. Ideally, the estimated RUL should always be within these error limits. The weighted mean oscillates around the true RUL until the end of life, and is only outside of the 30% error in a brief time between $t \approx [142, 152]$ hours.

(a)

(b)
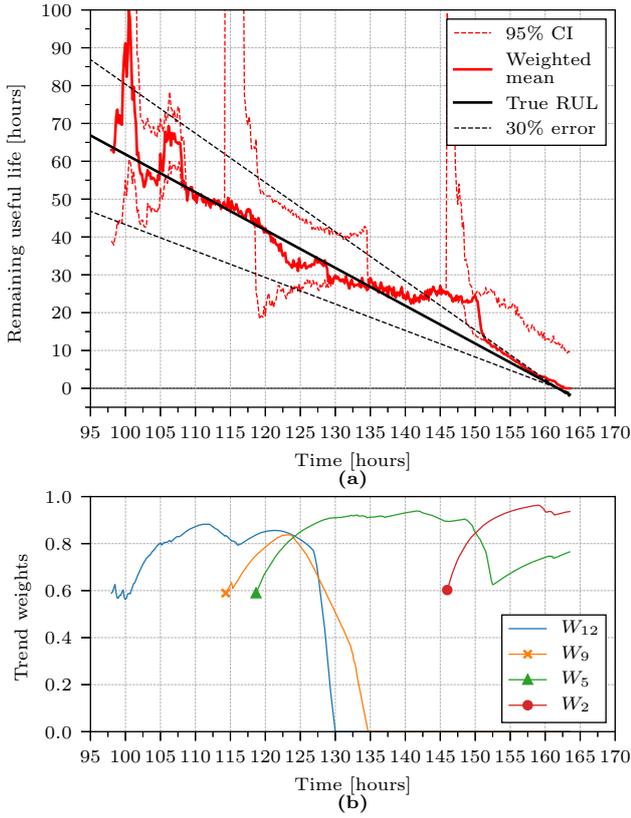
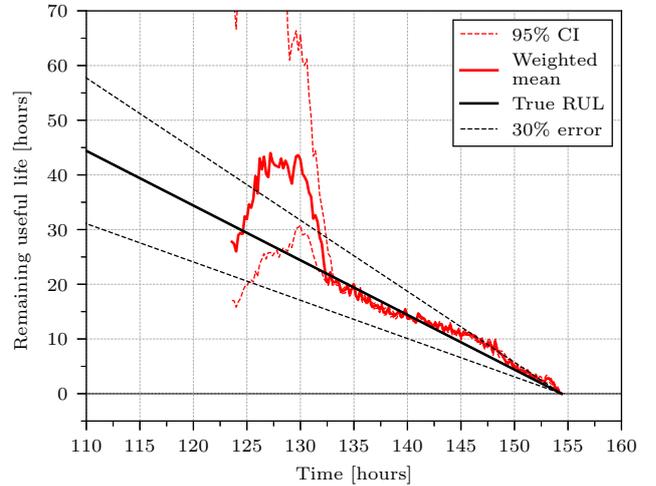Figure 5: Estimated RUL of the IMS dataset using the proposed method. (a) weighted mean, 95% CI, true RUL and 30% error margins; (b) weights for each PF prediction.

When $t = 125$ hours, three PFs have a similar weight as shown in Fig. 5 (b), because of their high Spearman coefficient. The weighted mean calculated using (41) is somewhere between these three RUL estimates, resulting in an estimate close to the true RUL. The lower 95% CI shows the lowest estimation of the trends and is considered a conservative estimate of the RUL. Afterward, the weights W_{12} and W_9 decrease towards 0 due to a low Spearman coefficient, and model predictions of R_5 and R_2 provide a reasonable estimate of the RUL.

5.2 Test rig 2 — in-house setup

Data from a second test rig is used to validate the proposed method further. A 6008-type roller element bearing is worn naturally in an accelerated life test by applying radial and axial loads. The dynamic capacity of the bearing is 17.8 kN, and the static capacity is 11 kN. With constant radial and axial loads of 9 kN and 5 kN, respectively, the bearing lasted approximately 34.6 million revolutions before failing due to an outer
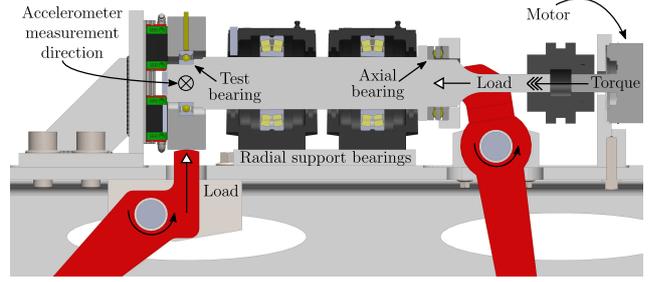
Figure 6: Test rig 2 Klausen et al. (2017a).

(a)

(b)
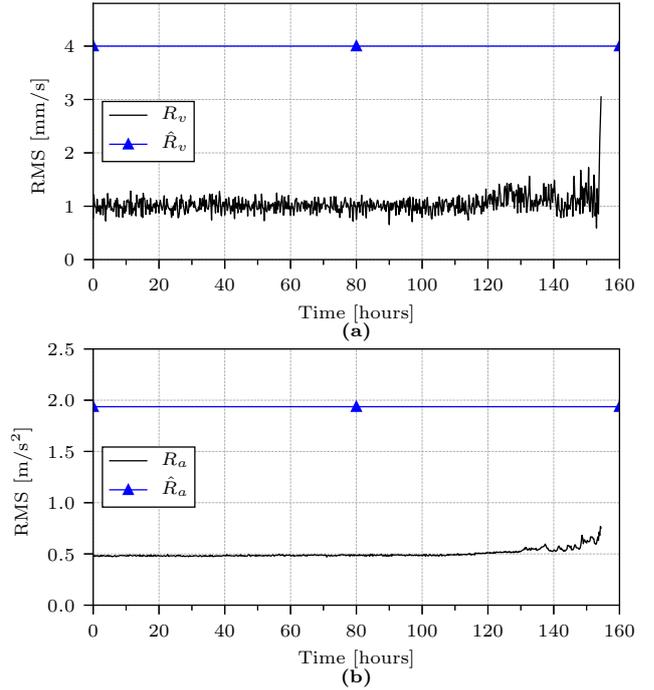
Figure 7: Comparison of velocity- and acceleration-based RMS of the in-house test rig dataset. (a) velocity-based RMS; (b) acceleration-based RMS.

race fault. The motor was operated at 700 rpm during measurements, and a planetary gearbox with a ratio of 1:7 caused the test bearing on the output shaft to rotate at 100 rpm. Vibration data was sampled every 12 minutes (5 times per hour) at 51200 Hz for 6 seconds. The 154 last hours of operation are used to verify the performance of the proposed method. The test rig is shown in Figure 6, and more details are given in Klausen et al. (2017a).

The velocity- and acceleration-based RMS are shown in Figs. 7 (a) and (b), respectively. The velocity-based FT is set to $\hat{R}_v = 4.0$ mm/s because a 1.1 kW motor is used, and the vibration signal was high-pass filtered at
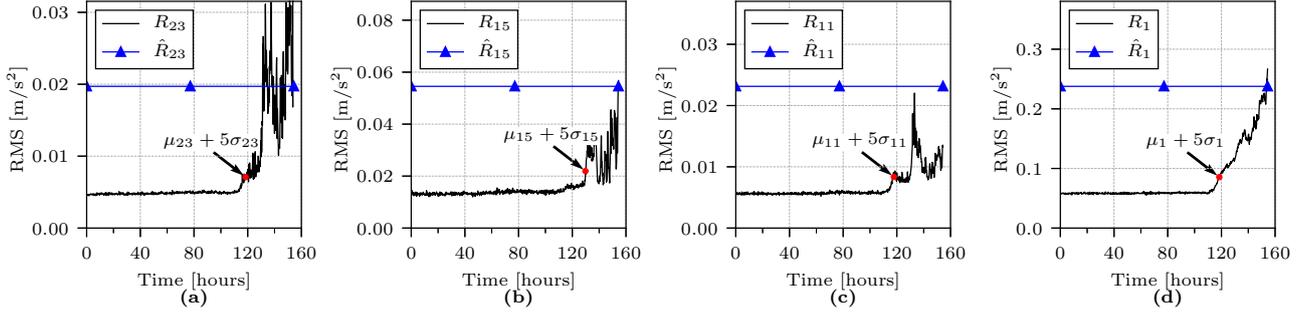
Figure 8: Collection of RMS trends with FTs for the in-house test rig dataset. (a) R_{23} [8800, 9200] Hz; (b) R_{15} [5600, 6000] Hz; (c) R_{11} [4000, 4400] Hz; (d) R_1 [0, 400] Hz.
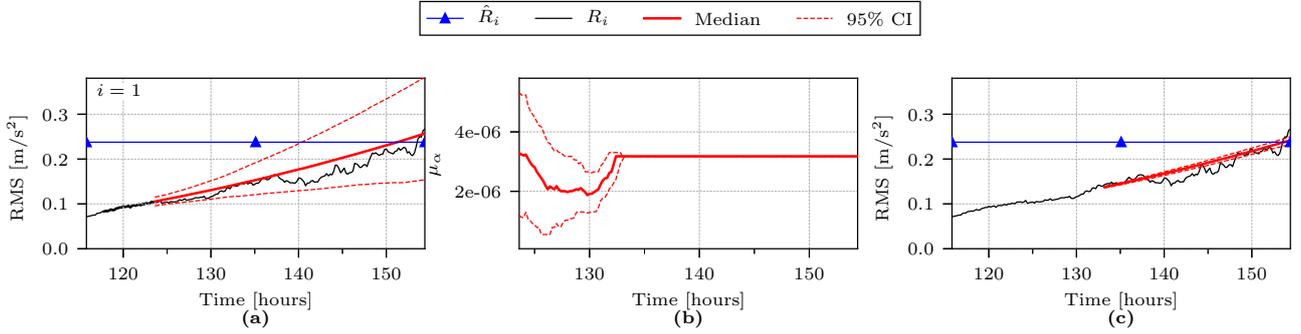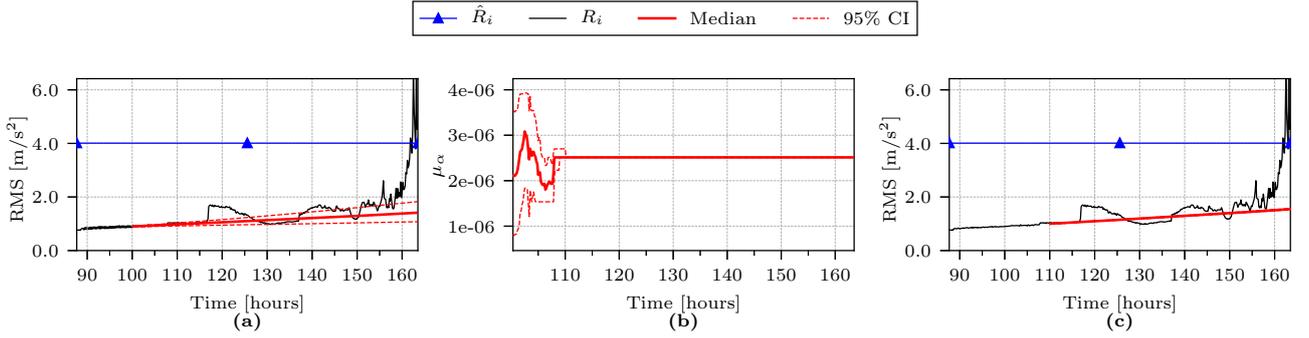

Figure 9: R_1 and initial median and 95% CI output of the corresponding PF. (a) R_1 with marked part as optimization input, blue line for FT, and red lines for median and 95% CI of PF; (b) α over time for the initiated PF; (c) predicted PF trend when μ_α converges.

Table 2: Initial PF parameter values for test rig 2 experiment.

	μ_α	σ_α^2	σ_h^2	β
PF_1	$3.21 \cdot 10^{-6}$	$1.14 \cdot 10^{-12}$	$2.25 \cdot 10^{-5}$	0.5

10 Hz because of the motor speed of 700 rpm. Other hyper-parameters (such as $\hat{\rho}$, N_p, ρ_L, etc.) are the same as in experimental test 1, except where noted in the following.

The velocity-FT $\hat{R}_v$ is almost reached at the end of useful life, as shown in Fig. 7 (a). On the other hand, the transformed acceleration-based FT $\hat{R}_a$ is far from reached in Fig. 7 (b). The test was stopped due to a high torque requirement, indicating the bearing was severely damaged. If the test was run for a few more measurement cycles, $\hat{R}_a$ might have been reached. Nevertheless, it is assumed that the end of life is the time of final measurement in this case.

The proposed method is used to split the vibration signal into $N_b = 25$ frequency bands, resulting in a frequency bandwidth of 400 Hz. Some of the RMS trends are shown in Fig. 8. R_{23} in Fig. 8 (a) is very noisy,

Figure 10: Estimated RUL of the in-house test rig dataset using the proposed method. The weighted mean, 95% CI, true RUL and 30% error margins are shown.

and hence not suitable for RUL estimation. Additionally, R_{15} and R_{11} in Figs. 8 (b) and (c) do not increase

33

Figure 11: R_1 and initial median and 95% CI output of the corresponding PF. (a) R_1 with marked part as optimization input, blue line for FT, and red lines for median and 95% CI of PF; (b) α over time for the initiated PF; (c) predicted PF trend when μ_α converges.

Table 3: Comparison of error. The best values are shown in bold.

	e_1	e_2
Proposed method *mean*	7.88	10.33
Proposed method *best*	**3.81**	6.25
PF on full RMS	142.96	144.78
PF on MD-based HI - Klausen et al. (2018)	22.64	25.14
Multi-scale approach - Qian et al. (2017)	4.61	**5.15**

steadily. R_1 in Fig. 8 (d), on the other hand, increases almost linearly after the degradation alarm is triggered, which makes the trend suitable for RUL estimation.

The first 30 hours in the dataset are used to calculate the baseline values. 5 hours data is utilized to determine the Spearman coefficient and optimization of initial values, e.g. $n_s = n_o = 25$. The first and only identified RMS trend is R_1 at $t = 116.5$ hours using the proposed RUL estimation algorithm. The initial PF parameters are given in Table 2. The initial PF output and R_1 are shown in Fig. 9 (a), and μ_α is shown in Fig. 9 (b). The trend is re-drawn in Fig. 9 (c) to show the PF prediction when μ_α has converged. Since the predicted trend is similar to new samples, the estimated RUL is accurate.

The weighted RUL in Fig. 10 is close to the actual RUL during the rest of the lifetime. The main reason is that R_1 increases almost linearly with time, and the final measurements are very close to the FT.

5.3 Comparisons

The proposed method's performance is compared to other methods that use RMS and do not rely on historical failure data. The performance is evaluated by
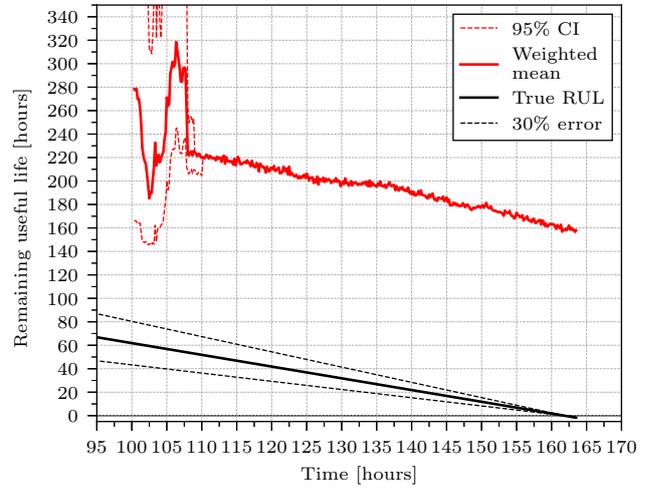
Figure 12: Estimated RUL of the IMS dataset using PF on RMS. The weighted mean, 95% CI, true RUL and 30% error margins are shown.

the average error and root mean square error using the following equations Qian et al. (2017):

$$e_1 = \frac{1}{M} \sum_{i=1}^{M} |\hat{l}_i - \tilde{l}_i| \qquad (42)$$

$$e_2 = \sqrt{\frac{1}{M} \sum_{i=1}^{M} (\hat{l}_i - \tilde{l}_i)^2} \qquad (43)$$

where $\hat{l}_i$ is the estimated RUL at index i (weighted mean of $p(\bar{l}_i|R_{1:N_b})$ in case of PF) and $\tilde{l}_i$ is the true RUL at index i. The range $i \in [1, M]$ corresponds to all the values for which the method estimates the RUL. The results from combining the proposed method with a Gaussian importance re-sampling PF are non-deterministic, meaning that runs with different random seeds produce slightly different results of e_1 and e_2.
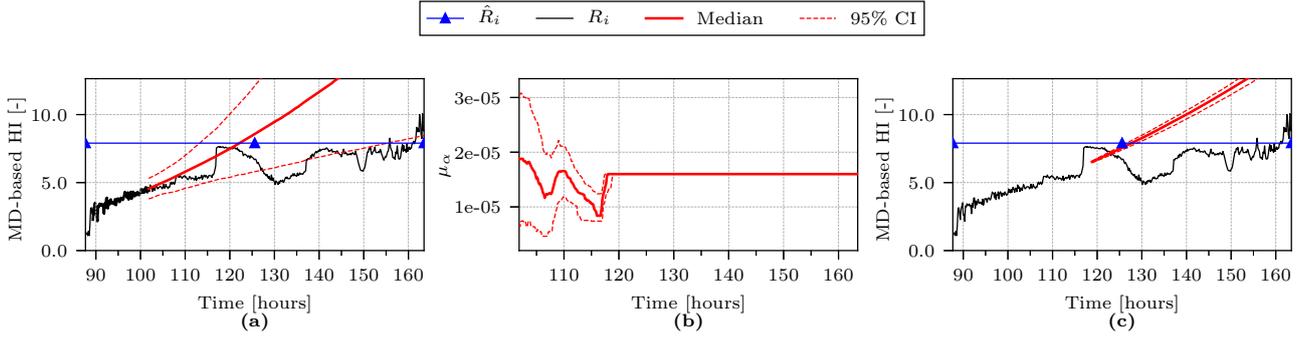
Figure 13: R_1 and initial median and 95% CI output of the corresponding PF. (a) R_1 with marked part as optimization input, blue line for FT, and red lines for median and 95% CI of PF; (b) α over time for the initiated PF; (c) predicted PF trend when μ_α converges.

Hence, the same RUL estimation as given in Section 5.1 is carried out 1000 times with different random seeds to acquire a mean value of error. The mean and minimum errors of the proposed method and comparisons are available in Table 3.

The first comparison utilizes the PF as described in Section 4.3 directly on the full RMS dataset. The initial degradation alarm is still determined based on the mean and STD of RMS value during the first 180 measurements. The results are shown in Fig. 11. The PF is initialized at $t \approx 100$ hours as seen in Fig. 11 (a), and the PF follows initial trend of the signal. However, once the PF converges at $t \approx 110$ hours, the PF output is not directed at the failure threshold, but rather below it, as shown in Fig. 11 (c). The result is an overestimated RUL, as is shown in Fig. 12. In this figure, the weighted mean of the PF is much greater than the true RUL. In effect, the error for this estimation is considerable, as pointed out in Table 3.

The second comparison utilizes the Mahalanobis-distance-based HI (MD-based HI) to create a more linear HI compared to standard RMS. The method of generating the HI is well described in Wang et al. (2016), and the FT for this HI is calculated using the method in Klausen et al. (2018). The PF with Paris' law is utilized to predict the RUL using this MD-based HI. The results are shown in Fig. 13. At roughly 100 hours, the PF is initialized as indicated in Fig. 13 (a). Once converged, the PF output is directed straight at the FT, as shown in Fig. 13 (c). This convergence results in a very conservative RUL estimation, as seen in Fig. 14. The error is lower than standard RMS, as shown in Table 3, but not as low as the proposed method.

The final comparison is the resulting RUL reported in Qian et al. (2017) for the IMS dataset. The error for this one is also given in Table 3. While e_2 is lower for the method given in Qian et al. (2017), it must be noted that the method described requires historical
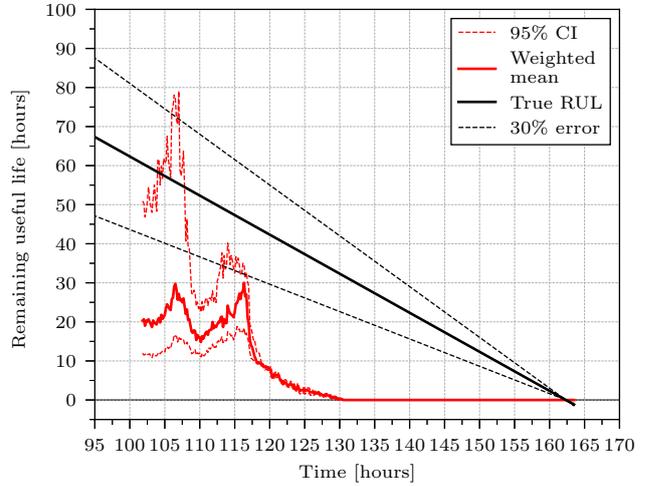

Figure 14: Estimated RUL of the IMS dataset using PF on MD-based HI. The weighted mean, 95% CI, true RUL and 30% error margins are shown.

failure data to work. This historical data is used to determine two parameters, namely D_1 and D_2 in Qian et al. (2017). Therefore, while the error can be compared between the proposed method and Qian et al. (2017), it should be noted that the proposed method does not require historical failure data.

6 Conclusions

This paper proposes a novel method for subdividing the vibration signal into multiple frequency bands for root mean square (RMS) calculations. The method utilizes a single discrete Fourier transform (DFT) per signal, and individual bins are used to acquire the signal energy within a frequency band. The Spearman coeffi-

cient identifies monotonic RMS trends suitable for the remaining useful life (RUL) estimation. It is observed that low-frequency RMS bands are most monotonic, while higher frequency RMS bands show earlier signs of degradation. The failure threshold (FT) for vibration RMS, developed in earlier research, has been extended for multiple RMS trends. A framework for combining the RUL estimation for each monotonic RMS trend has been presented. The Gaussian importance re-sampling particle filter (PF) is applied to determine the Paris' law parameters for estimating the RUL on two experimental tests. The results show that the proposed method produces reasonable RUL estimations without the use of historical failure data. The performance is comparable to another method reported in the literature that requires historical failure data.

References

Abboud, D., Elbadaoui, M., Smith, W., and Randall, R. Advanced bearing diagnostics: A comparative study of two powerful approaches. *Mechanical Systems and Signal Processing*, 2019. 114:604–627. doi:10.1016/j.ymssp.2018.05.011.

Ahmad, W., Khan, S. A., and Kim, J.-M. A Hybrid Prognostics Technique for Rolling Element Bearings Using Adaptive Predictive Models. *IEEE Transactions on Industrial Electronics*, 2018. 65(2):1577–1584. doi:10.1109/TIE.2017.2733487.

Akkad, K. and He, D. A Hybrid Deep Learning Based Approach for Remaining Useful Life Estimation. 2019. pages 1–6. doi:10.1109/ICPHM.2019.8819435.

An, D., Choi, J.-H., and Kim, N. H. Prognostics 101: A tutorial for particle filter-based prognostics algorithm using Matlab. *Reliability Engineering & System Safety*, 2013. 115:161–169. doi:10.1016/j.ress.2013.02.019.

An, H., Wang, G., Dong, Y., Yang, K., and Sang, L. Tool life prediction based on Gauss importance re-sampling particle filter. *The International Journal of Advanced Manufacturing Technology*, 2019. 103(9-12):4627–4634. doi:10.1007/s00170-019-03934-5.

Arulampalam, M., Maskell, S., Gordon, N., and Clapp, T. A tutorial on particle filters for online nonlinear/non-Gaussian Bayesian tracking. *IEEE Transactions on Signal Processing*, 2002. 50(2):174–188. doi:10.1109/78.978374.

Aye, S. and Heyns, P. An integrated Gaussian process regression for prediction of remaining useful life of slow speed bearings based on acoustic emission. *Mechanical Systems and Signal Processing*, 2017. 84:485–498. doi:10.1016/j.ymssp.2016.07.039.

Branch, M. A., Coleman, T. F., and Li, Y. A Subspace, Interior, and Conjugate Gradient Method for Large-Scale Bound-Constrained Minimization Problems. *SIAM Journal on Scientific Computing*, 1999. 21(1):1–23. doi:10.1137/s1064827595289108. Publisher: Society for Industrial & Applied Mathematics (SIAM).

Cheng, C., Ma, G., Zhang, Y., Sun, M., Teng, F., Ding, H., and Yuan, Y. A Deep Learning-Based Remaining Useful Life Prediction Approach for Bearings. *IEEE/ASME Transactions on Mechatronics*, 2020. 25(3):1243–1254. doi:10.1109/TMECH.2020.2971503. Conference Name: IEEE/ASME Transactions on Mechatronics.

Gebraeel, N., Lawley, M., Liu, R., and Parmeshwaran, V. Residual Life Predictions From Vibration-Based Degradation Signals: A Neural Network Approach. *IEEE Transactions on Industrial Electronics*, 2004. 51(3):694–700. doi:10.1109/TIE.2004.824875.

Hol, J. D., Schon, T. B., and Gustafsson, F. On Resampling Algorithms for Particle Filters. In *2006 IEEE Nonlinear Statistical Signal Processing Workshop*. IEEE, Cambridge, UK, pages 79–82, 2006. doi:10.1109/NSSPW.2006.4378824.

Hu, C., Youn, B. D., Wang, P., and Taek Yoon, J. Ensemble of data-driven prognostic algorithms for robust prediction of remaining useful life. *Reliability Engineering & System Safety*, 2012. 103:120–135. doi:10.1016/j.ress.2012.03.008.

ISO. Mechanical vibration Evaluation of machine vibration by measurements on non-rotating parts Part 3 (Standard no. 10816-3). 1998.

Khan, S. A., Prosvirin, A. E., and Kim, J.-M. Towards bearing health prognosis using generative adversarial networks: Modeling bearing degradation. In *2018 International Conference on Advancements in Computational Sciences (ICACS)*. IEEE, Lahore, pages 1–6, 2018. doi:10.1109/ICACS.2018.8333495.

Klausen, A., Folger, R. W., Robbersmyr, K. G., and Karimi, H. R. Accelerated Bearing Life-time Test Rig Development for Low Speed Data Acquisition. *Modeling, Identification and Control: A Norwegian Research Bulletin*, 2017a. 38(3):143–156. doi:10.4173/mic.2017.3.4.

Klausen, A., Robbersmyr, K. G., and Karimi, H. R. Autonomous Bearing Fault Diagnosis

Method based on Envelope Spectrum. *IFAC-PapersOnLine*, 2017b. 50(1):13378–13383. doi:10.1016/j.ifacol.2017.08.2262.

Klausen, A., Van Khang, H., and Robbersmyr, K. G. Novel Threshold Calculations for Remaining Useful Lifetime Estimation of Rolling Element Bearings. In *2018 XIII International Conference on Electrical Machines (ICEM)*. IEEE, Alexandroupoli, pages 1912–1918, 2018. doi:10.1109/ICELMACH.2018.8507056.

Lei, Y., Li, N., Gontarz, S., Lin, J., Radkowski, S., and Dybala, J. A Model-Based Method for Remaining Useful Life Prediction of Machinery. *IEEE Transactions on Reliability*, 2016a. 65(3):1314–1326. doi:10.1109/TR.2016.2570568.

Lei, Y., Li, N., Guo, L., Li, N., Yan, T., and Lin, J. Machinery health prognostics: A systematic review from data acquisition to RUL prediction. *Mechanical Systems and Signal Processing*, 2018. 104:799–834. doi:10.1016/j.ymssp.2017.11.016.

Lei, Y., Li, N., and Lin, J. A New Method Based on Stochastic Process Models for Machine Remaining Useful Life Prediction. *IEEE Transactions on Instrumentation and Measurement*, 2016b. 65(12):2671–2684. doi:10.1109/TIM.2016.2601004.

Li, N., Lei, Y., Lin, J., and Ding, S. X. An Improved Exponential Model for Predicting Remaining Useful Life of Rolling Element Bearings. *IEEE Transactions on Industrial Electronics*, 2015. 62(12):7762–7773. doi:10.1109/TIE.2015.2455055.

Lu, C., Chen, J., Hong, R., Feng, Y., and Li, Y. Degradation trend estimation of slewing bearing based on LSSVM model. *Mechanical Systems and Signal Processing*, 2016a. 76-77:353–366. doi:10.1016/j.ymssp.2016.02.031.

Lu, C., Wang, Y., Ragulskis, M., and Cheng, Y. Fault Diagnosis for Rotating Machinery: A Method based on Image Processing. *PLOS ONE*, 2016b. 11(10):e0164111. doi:10.1371/journal.pone.0164111.

Ma, M. and Mao, Z. Deep Recurrent Convolutional Neural Network for Remaining Useful Life Prediction. In *2019 IEEE International Conference on Prognostics and Health Management (ICPHM)*. pages 1–4, 2019. doi:10.1109/ICPHM.2019.8819440.

Manjurul Islam, M., Prosvirin, A. E., and Kim, J.-M. Data-driven prognostic scheme for rolling-element bearings using a new health index and variants of least-square support vector machines. *Mechanical Systems and Signal Processing*, 2021. 160:107853. doi:10.1016/j.ymssp.2021.107853.

McFadden, P. D. and Smith, J. D. Model for the vibration produced by a single point defect in a rolling element bearing. *Journal of Sound and Vibration*, 1984. 96(1):69–82. doi:10.1016/0022-460x(84)90595-9. Publisher: Elsevier BV.

Pan, Z., Meng, Z., Chen, Z., Gao, W., and Shi, Y. A two-stage method based on extreme learning machine for predicting the remaining useful life of rolling-element bearings. *Mechanical Systems and Signal Processing*, 2020. 144:106899. doi:10.1016/j.ymssp.2020.106899.

Paris, P. and Erdogan, F. A Critical Analysis of Crack Propagation Laws. *Journal of Basic Engineering*, 1963. 85(4):528–533. doi:10.1115/1.3656900. Publisher: ASME International.

Peeters, C., Guillaume, P., and Helsen, J. A comparison of cepstral editing methods as signal pre-processing techniques for vibration-based bearing fault detection. *Mechanical Systems and Signal Processing*, 2017. 91:354–381. doi:10.1016/j.ymssp.2016.12.036.

Qian, Y. and Yan, R. Remaining Useful Life Prediction of Rolling Bearings Using an Enhanced Particle Filter. *IEEE Transactions on Instrumentation and Measurement*, 2015. 64(10):2696–2707. doi:10.1109/TIM.2015.2427891.

Qian, Y., Yan, R., and Gao, R. X. A multi-time scale approach to remaining useful life prediction in rolling bearing. *Mechanical Systems and Signal Processing*, 2017. 83:549–567. doi:10.1016/j.ymssp.2016.06.031.

Qian, Y., Yan, R., and Hu, S. Bearing Degradation Evaluation Using Recurrence Quantification Analysis and Kalman Filter. *IEEE Transactions on Instrumentation and Measurement*, 2014. 63(11):2599–2610. doi:10.1109/TIM.2014.2313034.

Qiu, H., Lee, J., Lin, J., and Yu, G. Wavelet filter-based weak signature detection method and its application on rolling element bearing prognostics. *Journal of Sound and Vibration*, 2006. 289(4-5):1066–1090. doi:10.1016/j.jsv.2005.03.007.

Rycerz, P., Olver, A., and Kadiric, A. Propagation of surface initiated rolling contact fatigue cracks in bearing steel. *International Journal of Fatigue*, 2017. 97:29–38. doi:10.1016/j.ijfatigue.2016.12.004.

Singleton, R. K., Strangas, E. G., and Aviyente, S. Extended Kalman Filtering for Remaining-Useful-Life Estimation of Bearings. *IEEE Transactions on Industrial Electronics*, 2015. 62(3):1781–1790. doi:10.1109/TIE.2014.2336616.

Singleton, R. K., Strangas, E. G., and Aviyente, S. The Use of Bearing Currents and Vibrations in Lifetime Estimation of Bearings. *IEEE Transactions on Industrial Informatics*, 2017. 13(3):1301–1309. doi:10.1109/TII.2016.2643693.

Spearman, C. The Proof and Measurement of Association between Two Things. *The American Journal of Psychology*, 1904. 15(1):72. doi:10.2307/1412159. Publisher: JSTOR.

Wang, B., Lei, Y., Li, N., and Yan, T. Deep separable convolutional network for remaining useful life prediction of machinery. *Mechanical Systems and Signal Processing*, 2019. 134:106330. doi:10.1016/j.ymssp.2019.106330.

Wang, D. and Tsui, K.-L. Statistical Modeling of Bearing Degradation Signals. *IEEE Transactions on Reliability*, 2017. 66(4):1331–1344. doi:10.1109/TR.2017.2739126.

Wang, W. A model to predict the residual life of rolling element bearings given monitored condition information to date. *IMA Journal of Management Mathematics*, 2002. 13(1):3–16. doi:10.1093/imaman/13.1.3.

Wang, Y., Peng, Y., Zi, Y., Jin, X., and Tsui, K.-L. A Two-Stage Data-Driven-Based Prognostic Approach for Bearing Degradation Problem. *IEEE Transactions on Industrial Informatics*, 2016. 12(3):924–932. doi:10.1109/TII.2016.2535368.

Zhang, P., Du, Y., Habetler, T. G., and Lu, B. A Survey of Condition Monitoring and Protection Methods for Medium-Voltage Induction Motors. *IEEE Transactions on Industry Applications*, 2011. 47(1):34–46. doi:10.1109/TIA.2010.2090839.

Zhu, J., Chen, N., and Peng, W. Estimation of Bearing Remaining Useful Life Based on Multiscale Convolutional Neural Network. *IEEE Transactions on Industrial Electronics*, 2019. 66(4):3208–3216. doi:10.1109/TIE.2018.2844856.

Zhu, J., Chen, N., and Shen, C. A new data-driven transferable remaining useful life prediction approach for bearing under different working conditions. *Mechanical Systems and Signal Processing*, 2020. 139:106602. doi:10.1016/j.ymssp.2019.106602.